HHS Public Access
Author manuscript
Methods. Author manuscript; available in PMC 2017 September 16.

Published in final edited form as:
Methods. 2017 September 01; 128: 33–39. doi:10.1016/j.ymeth.2017.03.024.

Intravital imaging of the kidney

Takashi Hato[a,*], **Seth Winfree**[a], and **Pierre C. Dagher**[a,b,c,*]

[a]Department of Medicine, Indiana University, Indianapolis, IN, United States

[b]Department of Cellular and Integrative Physiology, Indiana University, Indianapolis, IN, United States

[c]Roudebush Indianapolis Veterans Affairs Medical Center, Indianapolis, IN, United States

Abstract

Two-photon intravital microscopy is a powerful tool that allows the examination of dynamic cellular processes in the live animal with unprecedented resolution. Indeed, it offers the ability to address unique biological questions that may not be solved by other means. While two-photon intravital microscopy has been successfully applied to study many organs, the kidney presents its own unique challenges that need to be overcome in order to optimize and validate imaging data. For kidney imaging, the complexity of renal architecture and salient autofluorescence merit special considerations as these elements directly impact image acquisition and data interpretation. Here, using illustrative cases, we provide practical guides and discuss issues that may arise during two-photon live imaging of the rodent kidney.

1. Introduction

The kidney is a highly complex organ that consists of more than 10 specialized epithelial cell types interlaced with numerous immune and interstitial cells as well as an organized vascular system. Intravital multiphoton microscopy studies conducted over the past 15 years have provided unique insights into kidney physiology and pathophysiology. However, there are many subtle issues commonly encountered that can complicate image acquisition when studying various aspects of kidney structure and function in the live animal. We have previously described in detail the basic surgical and microscopy platform we utilize for 2-photon imaging of the kidney [1–4]. We have also reported on the detailed use of various probes and delivery methods including advantages and limitations [5–15]. Therefore, in this review, we will focus on illustrating with examples specific aspects of 2-photon imaging of the kidneys including commonly encountered pitfalls and difficulties.

*Corresponding authors at: Division of Nephrology, 950 W Walnut Street, R2-202A, Indianapolis, IN 46202, United States. thato@iu.edu (T. Hato), pdaghe2@iupui.edu (P.C. Dagher).

Disclosures
None.

2. Materials and methods

All animal protocols were approved by Indiana University Institutional Animal Care Committee and conform to the National Institutes of Health Guide for the Care and Use of Laboratory Animals. Male C57BL/6J mice, B6129S1-Casp3^{tm1F1v}/J (caspase 3 knockout mice), B6;129S-Gt(ROSA)26Sor$^{tm1.1(CAG-COX8A/Dendra2)Dcc}$/J (photo-activatable mitochondria mice), B6.129P-Cx3cr1^{tm1Litt}/J (CX_3CR1-EGFP), and C57BL/6-Tg(CAG-EGFP)1Osb/J (all 8–10 weeks of age) were obtained from The Jackson Laboratory.

In some experiments, mice were subjected to a single dose of 5 mg/kg Alexa Fluor 568-labeled LPS from *S. minnesota* (Life Technologies and Sigma-Aldrich). Hoechst 33342 (Life Technologies), dissolved in normal saline, was administered intraperitoneally as a 2 mg/kg bolus 1–2 h before imaging. FITC-inulin (Sigma), a marker of tubular flow was administered intravenously (25 ng/kg). Tetramethylrhodamine methyl ester (TMRM, Life Technologies) was administered intravenously as a 10 μg/kg bolus from a DMSO stock diluted in normal saline. Phiphilux G2D2 (Calbiochem) 570 μl per mouse was injected iv through a jugular line and the kidney was imaged for periods up to 2 hours. The pH sensitive liposomes (DOPE/CHEMS) were a kind gift from Dr. Rudolph Juliano [16]. Approximately 80 mM of calcein was entrapped in 24 mM phospholipids. To remove free calcein, the liposomes were centrifuged (3000*g*) for 10 min immediately before use. The pellet was resuspended with 2 mL of TBS and 200 μl of the resuspended liposomes was injected via tail vein. E. coli were transformed with CFP plasmid (BL21 Star DE3 and pRSET/CFP, Life Technologies) and incubated in LB media until OD_{600} was achieved. Approximately $0.5x10^6$ CFU E coli were injected via tail vein.

Live animal imaging was performed using an Olympus FV1000-MPE confocal/multiphoton microscope equipped with a Spectra Physics MaiTai Deep See laser and gallium arsenide detectors, with signal digitized to 12 bit resolution. The system is mounted on an Olympus Ix81 inverted microscope stand with an Olympus 20× and 60× NA 1.2 water-immersion objective [17]. For most experiments, the laser was tuned to 800 nm wavelength. Animals were placed on the stage with the exposed intact kidney placed in a coverslip-bottomed cell culture dish (HBSt-5040; Warner Instruments) bathed in isotonic saline. Two ReptiTherm pads (Zoo Med) and a heated water jacket blanket were used to maintain the temperature at 36 °C.

3. Results and discussion

A typical two-photon microscopy setup (non-descanned detector) allows us to image a rodent kidney down to about 100 μm in depth from the renal capsule (Fig. 1A). Because of strong light scattering, deeper live imaging is currently limited as compared to other organs such as the brain, where less scattering species are present [1,18,19]. Improving imaging depth can be achieved with: 1) an increment in laser power, 2) the use of a high numerical aperture of the objective lens with matched refractive indices of the sample and immersion medium, 3) a long free working distance (e.g., Olympus objectives: XLPLanN 25x/1.05W MP, UPlanSApo 30x/1.05 Silicon oil, XLUMPlanFI 20x/0.95 W), 4) longer excitation

wavelength as achieved with an optical parametric oscillator [20,21]. These approaches have been used with variable success and will not be discussed further in this review.

4. Harnessing autofluorescence

Tissue autofluorescence may be problematic because it can overlap with the emission of commonly used probes. However, it can also be harnessed to define various structures in the field under examination. Fig. 1B shows a typical appearance of mouse kidney cortex. Note the presence of abundant proximal tubules (PT) recognized by their thickness and strong autofluorescence. Distal tubules, collecting ducts and thick ascending limbs are also seen as thinner tubules with dimmer autofluorescence. Surface cortical glomeruli are scarce especially in an adult mouse [22]. Importantly, note the presence of two distinct populations of PT segments, one with fine bright green punctate autofluorescence and the other with coarse red-green (appearing as brown color) autofluorescence. These two populations of PT segments represent S1 and S2 tubules, known to differ in their metabolic profiles and hence, their autofluorescence. To distinguish upstream S1 from downstream S2 segments, we followed the sequential appearance of systemically injected fluorescently-labeled inulin (Fig. 1B–D). All experiments confirmed that the tubules with red-green coarse autofluorescence are indeed upstream S1 while the tubules with fine bright green autofluorescence are downstream S2 [13]. Thus, autofluorescence can be useful in defining the various structures in the cortex without the use of exogenous probes.

5. Time-lapse imaging

Prolonged time-lapse imaging offers the ability to capture “slow” dynamic cellular changes that may not be otherwise apparent. Here we present two examples that highlight the power of extended kidney imaging. In Fig. 2A and B we show the dynamic development of acute tubular necrosis observed over 75 min (see also Supplemental Video 1). Note the flattening of the lining epithelium, swelling of the lumen and shedding of epithelial cells. These dynamic changes at subcellular resolution cannot be appreciated with short imaging times. Another example involves the trafficking of immune cells in the renal interstitium. The kidney hosts a breadth of immune cells that participate in the pathophysiology of a variety of renal diseases. The way in which immune cells interact with each other and with other renal structures is poorly understood. Using a transgenic mouse that expresses eGFP in all cell types and treated with endotoxin, we imaged a renal cortical field over a one hour time period. Note the trafficking of immune cells and their interactions with tubules and glomerular structures (Fig. 2C–E; Supplemental Video 2). These are likely slow moving macrophages and their activity can be easily missed with shorter imaging times.

6. Fluorescent probes

Fluorescent probes have been used extensively to characterize and image cellular processes *in vitro*. However, the *in vivo* use of these probes is met with unique challenges primarily related to probe delivery and distribution. Furthermore, many probes require strict microenvironmental physico-chemical parameters for optimal fluorescence. These can be easily set *in vitro* but much harder to control *in vivo*. In the kidney, the complex cellular

architecture, glomerular filtration barrier and vigorous PT endocytosis further dictate that very careful consideration be given to the selection of fluorescent probes for intravital imaging. Commonly used primary probes for intravital renal imaging are listed in Table 1. A number of secondary probes (endogenous or exogenous molecules conjugated to fluorescent probes) are also used to image various processes in the kidney after systemic injection. Finally, the list of transgenic animals with fluorescent indicators continues to grow. Some of the genetically encoded probes have the advantage of bypassing the technical difficulties associated with *in vivo* probe use we discuss here [23–25].

6.1. Molecular size and fluid phase uptake

We first address the importance of probe size. Because of the size selectivity of the glomerulus, a large molecular probe will not be filtered (typically >40 Kd or >4 nm) [26,27]. Conversely, smaller probes are freely filtered and readily appear in the urinary lumen. Thus, the half-life of a large probe in the circulation is generally much longer than that of a small molecular probe. This size difference can be harnessed to measure parameters such as glomerular filtration rate (GFR), blood and tubular flow. For example, we used high-molecular weight poly (I:C) (not filtered) to label Toll Like Receptor 3 (TLR3) positive immune cells in the circulation and interstitial space [17] (Fig. 6A). The use of low-molecular weight poly (I:C) could lead to low labeling efficiency due to the probe loss in the urinary lumen as a function of GFR. For filtered probes, the possible presence of PT fluid-phase and/or receptor mediated endocytosis requires additional consideration. For example, internalized probes may get decomposed or quenched in the endosomal/lysosomal compartment resulting in an underestimation of the reabsorption magnitude [7].

It is possible to distinguish fluid-phase from receptor-mediated endocytosis. This is done traditionally by analyzing the kinetics and co-localization of the probe with a known fluid-phase markers such as low molecular weight dextran [13]. In addition, if a transgenic knockout mouse is available for that particular receptor, it can be used to estimate the residual fluid-phase reabsorption component. We made use of such a model to distinguish the two components of endotoxin uptake in the PT. In Fig. 3A, we show that systemically administered Alexa-labeled endotoxin is internalized primarily by S1 proximal tubules in wild-type mice. In a TLR4 knockout mouse, we documented the presence of residual mild endotoxin uptake (Fig. 3B). This residual uptake likely represents receptor-independent fluid phase endocytosis [13].

6.2. Nonspecific probe signal

Exogenous probes are administered for the purpose of reporting on or detecting certain events in the organ or tissue of interest. However, for a variety of poorly understood reasons, non-specific probe activation can occur in the living organism. Therefore, it is important to always try and validate the signal when possible. As an example, we report on the use of the caspase 3 sensor Phiphilux G2D2. This probe is widely used *in vitro* to detect caspase 3 activity in apoptotic cells. Upon cleavage by caspase 3, this probe emits bright red fluorescence. When administered *in vivo* to uninjured wildtype mice, we noted the presence of diffuse red fluorescence at the apical border of S1 tubules (Fig. 3C). While this was unlikely to represent true apoptosis in these uninjured tubules, it raised the possibility of

apoptosis-independent caspase 3 activity in the highly dynamic brush border. However, when injected into a caspase 3 KO mouse, Phiphilux G2D2 exhibited a similar strong S1 apical fluorescence (Fig. 3D). This indicated non-specific, caspase-3-independent activation of the probe [28]. The origin of this activation remains unknown.

6.3. Heterogeneous probe distribution

The kidney is a highly metabolic organ and its metabolism is supported by an abundant mitochondrial network. Tetramethylrhodamine (TMRM) is a commonly used probe to monitor mitochondrial membrane potential. We and others have successfully used TMRM and other mitochondrial probes in live animals (Fig. 4A) [5,13]. However, in the case of TMRM, a heterogeneous distribution of the probe among various renal tubules is frequently observed. In fact, differential fluorescence can be even seen within the same tubule. It is unclear if this represents true heterogeneity in mitochondrial potential (related to different metabolic states) among various tubular subsegments or rather, a consequence of heterogeneous probe delivery due to focal microcirculatory failure (Fig. 4B) [29,30]. Note also that TMRM is completely absent from interstitial cells thus hindering the study of their mitochondrial potential (Fig. 4C, D).

6.4. Free dye

Renal resident macrophages play important roles in health and disease. A variety of probes can be directed to the macrophage population by harnessing their phagocytic activity. For example, liposomal clodronate is a popular means to target clodronate to the macrophage thus inducing apoptosis [31]. Similarly, liposomes loaded with fluorescent probes can be used as a vehicle to deliver the probes to macrophages (Fig. 5A, B; Calcein-liposomes). It is important to remove leaked free probe with dialysis or centrifugation before injecting the liposomes into the animal. Fig. 5C–E show the potential confounding effect of free dye. Calcein-liposomes were injected into the animal without strict removal of free dye. Note the markedly different distribution pattern compared to that in Fig. 5A–B. Free calcein was secreted into the urinary lumen primarily by S2 proximal tubules where Multi Drug Resistance 1 transporter is expressed. Calcein is a substrate for the transporter [32].

7. Analytical tools and software

Prolonged time-lapse imaging requires close monitoring of the animal under anesthesia. We use isoflurane rather than injectable anesthetics so that the anesthesia dose can be finely titrated and motion artifacts minimized. However, a drift of the imaging field and motion artifacts can still occur and make data interpretation rather problematic. In such cases, acquired imaging data can be salvaged using one of several freely available software to correct for motion artifacts. Fig. 6A, B and Supplemental Video 3 show an example in which motion artifact is reduced sequentially using Intravital Microscopy Artifact Reduction Tool software (IMART; rigid registration, non-rigid registration) [33]. In addition, there are multiple tools available for tracking moving cells in a 2D space, enabling quantitative analysis of cell trafficking. In Fig. 6C, D and Supplemental Video 4, we show such an example using an ImageJ plug-in we developed [17]. This plug-in defines moving objects based on size and highlights the actual path of the moving object with a time-graded color

tracing. Finally, commercially available software such as IMARIS can provide advanced volumetric rendering as well as 3D time series analysis (Fig. 6E) [34].

8. Conclusion

Here we presented multiple examples to illustrate the power of two-photon intravital microscopy. We also demonstrated select examples to underscore issues that are commonly encountered during intravital imaging of the kidney. The majority of commercially available fluorescent probes have not been tested for intravital microscopy. Understanding renal physiology and using proper controls are crucial to establish a reproducible experimental system. We did not discuss the use of plasmids or viruses as a means to deliver probes to the kidney because of the lack of established methods to date [10,35–40]. A simple injection of plasmids (via tail vein or jugular vein) is not effective due to trapping by other organs. Commonly used viruses such as lentivirus or adeno-associated viruses do not have tropism to the kidney [41]. In the era of genome-editing with the CRISPR system *in vivo* [42,43], it has become even more important to optimize and refine renal targeting methods. Hopefully, this bottleneck problem will be overcome in the near future with the emergence of exciting next-generation intracellular delivery technologies [44,45].

Supplementary Material

Refer to Web version on PubMed Central for supplementary material.

Acknowledgments

This work was supported by NIH grant R01-DK107623, VA Merit (1I01BX002901), NIH O'Brien Center grant P30-DK079312 to P.C.D., Paul Teschan Research grant (Dialysis Clinics Inc.), Indiana Clinical and Translational Sciences Institute grant (KL2TR001106) to T.H. IMART was obtained from the Indiana O'Brien Center for Advanced Microscopic Analysis, which is supported by funding from the National Institutes of Health NIH/NIDDK P50 DK61594.

References

1. Dunn KW, Sandoval RM, Kelly KJ, Dagher PC, Tanner GA, Atkinson SJ, Bacallao RL, Molitoris BA. Functional studies of the kidney of living animals using multicolor two-photon microscopy. Am J Physiol Cell Physiol. 2002; 283(3):C905–C916. [PubMed: 12176747]
2. Dunn KW, Sutton TA, Sandoval RM. Live-animal imaging of renal function by multiphoton microscopy. Curr Protoc Cytom. 2012; chapter 14(Unit 12.9)
3. Molitoris BA, Sandoval RM. Multiphoton imaging techniques in acute kidney injury. Contrib Nephrol. 2010; 165:46–53. [PubMed: 20427955]
4. Molitoris BA, Sandoval RM. Techniques to study nephron function: microscopy and imaging. Pflügers Arch. 2009; 458(1):203–209. [PubMed: 19145447]
5. Hall AM, Rhodes GJ, Sandoval RM, Corridon PR, Molitoris BA. In vivo multiphoton imaging of mitochondrial structure and function during acute kidney injury. Kidney Int. 2013; 83(1):72–83. [PubMed: 22992467]
6. Sandoval RM, Wagner MC, Patel M, Campos-Bilderback SB, Rhodes GJ, Wang E, Wean SE, Clendenon SS, Molitoris BA. Multiple factors influence glomerular albumin permeability in rats. J Am Soc Nephrol. 2012; 23(3):447–457. [PubMed: 22223875]
7. Sandoval RM, Kennedy MD, Low PS, Molitoris BA. Uptake and trafficking of fluorescent conjugates of folic acid in intact kidney determined using intravital two-photon microscopy. Am J Physiol Cell Physiol. 2004; 287(2):C517–C526. [PubMed: 15102609]

8. Sandoval RM, Wang E, Molitoris BA. Finding the bottom and using it: offsets and sensitivity in the detection of low intensity values in vivo with 2-photon microscopy. Intravital. 2014; 2(1)
9. Collett JA, Corridon PR, Mehrotra P, Kolb AL, Rhodes GJ, Miller CA, Molitoris BA, Pennington JG, Sandoval RM, Atkinson SJ, Campos-Bilderback SB, Basile DP, Bacallao RL. Hydrodynamic Isotonic Fluid Delivery Ameliorates Moderate-to-Severe Ischemia-Reperfusion Injury in Rat Kidneys. J Am Soc Nephrol. 2017
10. Corridon PR, Rhodes GJ, Leonard EC, Basile DP, Gattone VH 2nd, Bacallao RL, Atkinson SJ. A method to facilitate and monitor expression of exogenous genes in the rat kidney using plasmid and viral vectors. Am J Physiol Renal Physiol. 2013; 304(9):F1217–F1229. [PubMed: 23467422]
11. Choong FX, Sandoval RM, Molitoris BA, Richter-Dahlfors A. Multiphoton microscopy applied for real-time intravital imaging of bacterial infections in vivo. Methods Enzymol. 2012; 506:35–61. [PubMed: 22341218]
12. Tanner GA, Sandoval RM, Molitoris BA, Bamburg JR, Ashworth SL. Micropuncture gene delivery and intravital two-photon visualization of protein expression in rat kidney. Am J Physiol Renal Physiol. 2005; 289(3):F638–F643. [PubMed: 15886277]
13. Kalakeche R, Hato T, Rhodes G, Dunn KW, El-Achkar TM, Plotkin Z, Sandoval RM, Dagher PC. Endotoxin uptake by S1 proximal tubular segment causes oxidative stress in the downstream S2 segment. J Am Soc Nephrol. 2011; 22(8):1505–1516. [PubMed: 21784899]
14. Hato T, Winfree S, Day R, Sandoval RM, Molitoris BA, Yoder MC, Wiggins RC, Zheng Y, Dunn KW, Dagher PC. Two-photon intravital fluorescence lifetime imaging of the kidney reveals cell-type specific metabolic signatures. J Am Soc Nephrol. 2017
15. Ashworth SL, Sandoval RM, Tanner GA, Molitoris BA. Two-photon microscopy: visualization of kidney dynamics. Kidney Int. 2007; 72(4):416–421. [PubMed: 17538570]
16. Juliano RL. A personal reflection on the career of the 2004 Life-time Achievement Award winner. J Drug Target. 2004; 12(6):313–314. [PubMed: 15545081]
17. Hato T, Winfree S, Kalakeche R, Dube S, Kumar R, Yoshimoto M, Plotkin Z, Dagher PC. The macrophage mediates the renoprotective effects of endotoxin preconditioning. J Am Soc Nephrol. 2015; 26(6):1347–1362. [PubMed: 25398784]
18. Peti-Peterdi J, Kidokoro K, Riquier-Brison A. Novel in vivo techniques to visualize kidney anatomy and function. Kidney Int. 2015; 88(1):44–51. [PubMed: 25738253]
19. Helmchen F, Denk W. Deep tissue two-photon microscopy. Nat Methods. 2005; 2(12):932–940. [PubMed: 16299478]
20. Kobat D, Durst ME, Nishimura N, Wong AW, Schaffer CB, Xu C. Deep tissue multiphoton microscopy using longer wavelength excitation. Opt Express. 2009; 17(16):13354–13364. [PubMed: 19654740]
21. Clendenon SG, Young PA, Ferkowicz M, Phillips C, Dunn KW. Deep tissue fluorescent imaging in scattering specimens using confocal microscopy. Microsc Microanal. 2011; 17(4):614–617. [PubMed: 21729357]
22. Schiessl IM, Bardehle S, Castrop H. Superficial nephrons in BALB/c and C57BL/6 mice facilitate in vivo multiphoton microscopy of the kidney. PLoS One. 2013; 8(1):e52499. [PubMed: 23349687]
23. Szebenyi K, Furedi A, Kolacsek O, Csohany R, Prokai A, Kis-Petik K, Szabo A, Bosze Z, Bender B, Tovari J, Enyedi A, Orban TI, Apati A, Sarkadi B. Visualization of calcium dynamics in kidney proximal tubules. J Am Soc Nephrol. 2015; 26(11):2731–2740. [PubMed: 25788535]
24. Burford JL, Villanueva K, Lam L, Riquier-Brison A, Hackl MJ, Pippin J, Shankland SJ, Peti-Peterdi J. Intravital imaging of podocyte calcium in glomerular injury and disease. J Clin Invest. 2014; 124(5):2050–2058. [PubMed: 24713653]
25. Hackl MJ, Burford JL, Villanueva K, Lam L, Susztak K, Schermer B, Benzing T, Peti-Peterdi J. Tracking the fate of glomerular epithelial cells in vivo using serial multiphoton imaging in new mouse models with fluorescent lineage tags. Nat Med. 2013; 19(12):1661–1666. [PubMed: 24270544]
26. Brenner BM, Hostetter TH, Humes HD. Molecular basis of proteinuria of glomerular origin. N Engl J Med. 1978; 298(15):826–833. [PubMed: 634317]

27. Ruggiero A, Villa CH, Bander E, Rey DA, Bergkvist M, Batt CA, Manova-Todorova K, Deen WM, Scheinberg DA, McDevitt MR. Paradoxical glomerular filtration of carbon nanotubes. Proc Natl Acad Sci USA. 2010; 107(27):12369–12374. [PubMed: 20566862]
28. Hato T, Sandoval R, Dagher PC. The caspase 3 sensor Phiphilux G2D2 is activated non-specifically in S1 renal proximal tubules. Intravital. 2015; 4(2)
29. Nakano D, Doi K, Kitamura H, Kuwabara T, Mori K, Mukoyama M, Nishiyama A. Reduction of tubular flow rate as a mechanism of oliguria in the early phase of endotoxemia revealed by intravital imaging. J Am Soc Nephrol. 2015; 26(12):3035–3044. [PubMed: 25855781]
30. Hall AM, Crawford C, Unwin RJ, Duchen MR, Peppiatt-Wildman CM. Multiphoton imaging of the functioning kidney. J Am Soc Nephrol. 2011; 22(7):1297–1304. [PubMed: 21719788]
31. Ferenbach DA, Sheldrake TA, Dhaliwal K, Kipari TM, Marson LP, Kluth DC, Hughes J. Macrophage/monocyte depletion by clodronate, but not diphtheria toxin, improves renal ischemia/reperfusion injury in mice. Kidney Int. 2012; 82(8):928–933. [PubMed: 22673886]
32. Essodaigui M, Broxterman HJ, Garnier-Suillerot A. Kinetic analysis of calcein and calcein-acetoxymethylester efflux mediated by the multidrug resistance protein and P-glycoprotein. Biochemistry. 1998; 37(8):2243–2250. [PubMed: 9485370]
33. Dunn KW, Lorenz KS, Salama P, Delp EJ. IMART software for correction of motion artifacts in images collected in intravital microscopy. Intravital. 2014; 3(1):e28210. [PubMed: 26090271]
34. Deforet M, Parrini MC, Petitjean L, Biondini M, Buguin A, Camonis J, Silberzan P. Automated velocity mapping of migrating cell populations (AVeMap). Nat Methods. 2012; 9(11):1081–1083. [PubMed: 23064519]
35. Espana-Agusti J, Tuveson DA, Adams DJ, Matakidou A. A minimally invasive, lentiviral based method for the rapid and sustained genetic manipulation of renal tubules. Sci Rep. 2015; 5:11061. [PubMed: 26046460]
36. Gusella GL, Fedorova E, Marras D, Klotman PE, Klotman ME. In vivo gene transfer to kidney by lentiviral vector. Kidney Int. 2002; 61(1 Suppl):S32–S36. [PubMed: 11841609]
37. Kim M, Chen SW, Park SW, Kim M, D'Agati VD, Yang J, Lee HT. Kidney-specific reconstitution of the A1 adenosine receptor in A1 adenosine receptor knockout mice reduces renal ischemia-reperfusion injury. Kidney Int. 2009; 75(8):809–823. [PubMed: 19190680]
38. Rocca CJ, Ur SN, Harrison F, Cherqui S. RAAV9 combined with renal vein injection is optimal for kidney-targeted gene delivery: conclusion of a comparative study. Gene Ther. 2014; 21(6):618–628. [PubMed: 24784447]
39. Kurosaki T, Kawakami S, Higuchi Y, Suzuki R, Maruyama K, Sasaki H, Yamashita F, Hashida M. Kidney-selective gene transfection using anionic bubble lipopolyplexes with renal ultrasound irradiation in mice. Nanomedicine. 2014; 10(8):1829–1838. [PubMed: 24954382]
40. Mukai H, Kawakami S, Hashida M. Renal press-mediated transfection method for plasmid DNA and siRNA to the kidney. Biochem Biophys Res Commun. 2008; 372(3):383–387. [PubMed: 18445481]
41. Nakayama M, Both GW, Banizs B, Tsuruta Y, Yamamoto S, Kawakami Y, Douglas JT, Tani K, Curiel DT, Glasgow JN. An adenovirus serotype 5 vector with fibers derived from ovine atadenovirus demonstrates CAR-independent tropism and unique biodistribution in mice. Virology. 2006; 350(1):103–115. [PubMed: 16516257]
42. Platt RJ, Chen S, Zhou Y, Yim MJ, Swiech L, Kempton HR, Dahlman JE, Parnas O, Eisenhaure TM, Jovanovic M, Graham DB, Jhunjhunwala S, Heidenreich M, Xavier RJ, Langer R, Anderson DG, Hacohen N, Regev A, Feng G, Sharp PA, Zhang F. CRISPR-Cas9 knockin mice for genome editing and cancer modeling. Cell. 2014; 159(2):440–455. [PubMed: 25263330]
43. Miyagi A, Lu A, Humphreys BD. Gene editing: powerful new tools for nephrology research and therapy. J Am Soc Nephrol. 2016; 27(10):2940–2947. [PubMed: 27358322]
44. Stewart MP, Sharei A, Ding X, Sahay G, Langer R, Jensen KF. In vitro and ex vivo strategies for intracellular delivery. Nature. 2016; 538(7624):183–192. [PubMed: 27734871]
45. Bidwell, GL., 3rd, Mahdi, F., Shao, Q., Logue, OC., Waller, JP., Reese, C., Chade, AR. A kidney-selective biopolymer for targeted drug delivery. Am J Physiol Renal Physiol. 2016. http://dx.doi.org/10.1152/ajprenal.00143.2016

46. Horbelt M, Wotzlaw C, Sutton TA, Molitoris BA, Philipp T, Kribben A, Fandrey J, Pietruck F. Organic cation transport in the rat kidney in vivo visualized by time-resolved two-photon microscopy. Kidney Int. 2007; 72(4):422–429. [PubMed: 17495857]

47. Brasen JC, Burford JL, McDonough AA, Holstein-Rathlou NH, Peti-Peterdi J. Local pH domains regulate NHE3-mediated Na(+) reabsorption in the renal proximal tubule. Am J Physiol Renal Physiol. 2014; 307(11):F1249–F1262. [PubMed: 25298526]

48. Tanner GA, Sandoval RM, Dunn KW. Two-photon in vivo microscopy of sulfonefluorescein secretion in normal and cystic rat kidneys. Am J Physiol Renal Physiol. 2004; 286(1):F152–F160. [PubMed: 12965895]

Appendix A. Supplementary data

Supplementary data associated with this article can be found, in the online version, at http://dx.doi.org/10.1016/j.ymeth.2017.03.024.

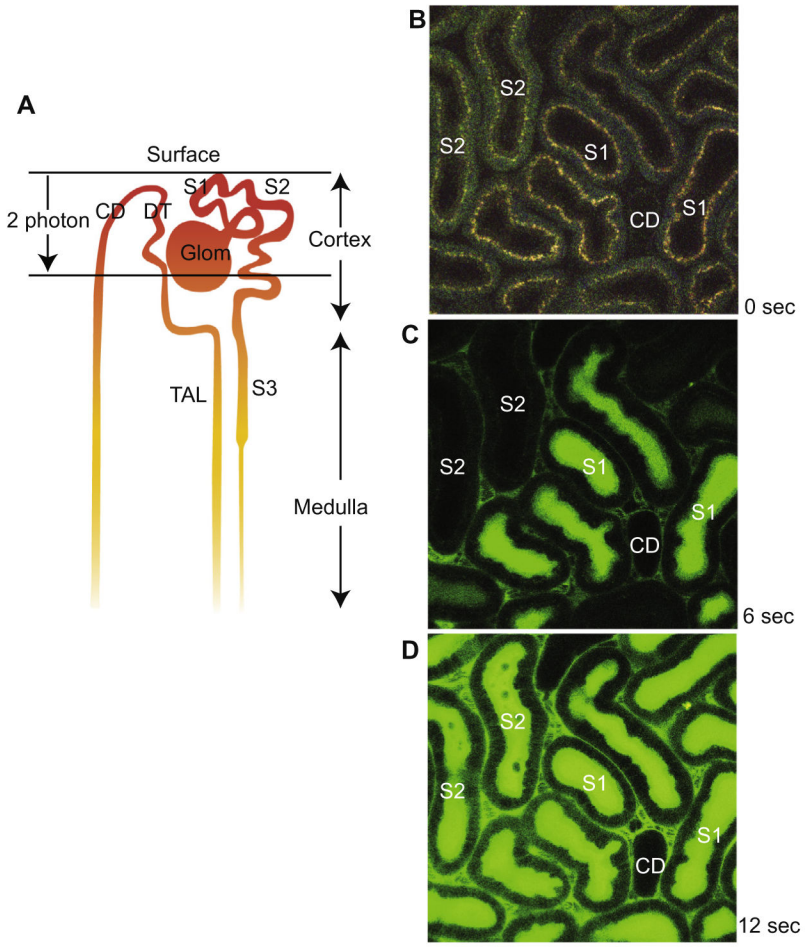

Fig. 1.

Identification of renal tubule segments with intravital two-photon microscopy. (A) Schematic nephron structure and subsegments are shown. S3 proximal tubules are located at depths beyond the reach of 2 photon microscopy. DT; distal tubule, CD; collecting duct, TAL; thick ascending limb of loop of Henle. (B) Intravital 2 photon microscopy of mouse kidney cortex. S1 proximal tubules exhibit coarse red-green autofluorescence whereas S2 tubules have fine bright green punctate autofluorescence. (C and D) FITC-labeled inulin appears sequentially in S1 and S2 segments. (For interpretation of the references to colour in this figure legend, the reader is referred to the web version of this article.)

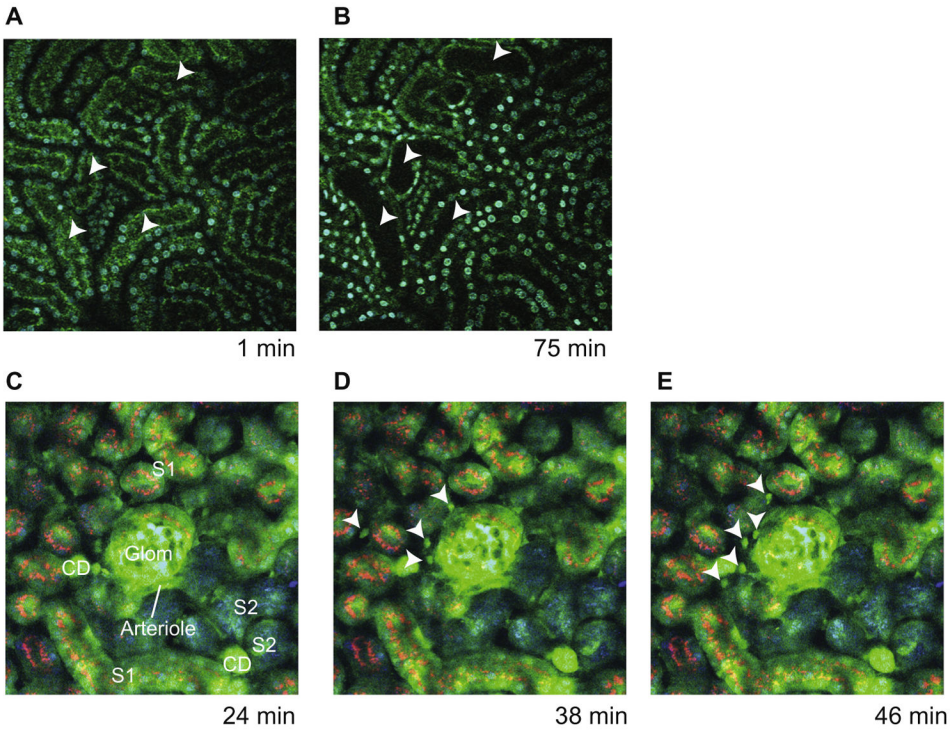

Fig. 2.

Dynamic changes captured by prolonged time-lapse imaging. (A and B) Intravital imaging of ischemic mouse kidney. The kidney was imaged every 9 s over 75 min. Nuclei are labeled blue with Hoechst. Arrowheads point to flattening of epithelial lining of proximal tubules concomitant with luminal swelling. See Supplemental video 1. Note that the TMRM signal seen in the video was not shown in the still frames of Fig. 2 for clarity. (C–E) Time-lapse imaging of myeloid cells (arrowheads; green) after Alexa-labeled endotoxin treatment (red) in transgenic mice that express eGFP in all cell types. See Supplemental video 2. (For interpretation of the references to colour in this figure legend, the reader is referred to the web version of this article.)

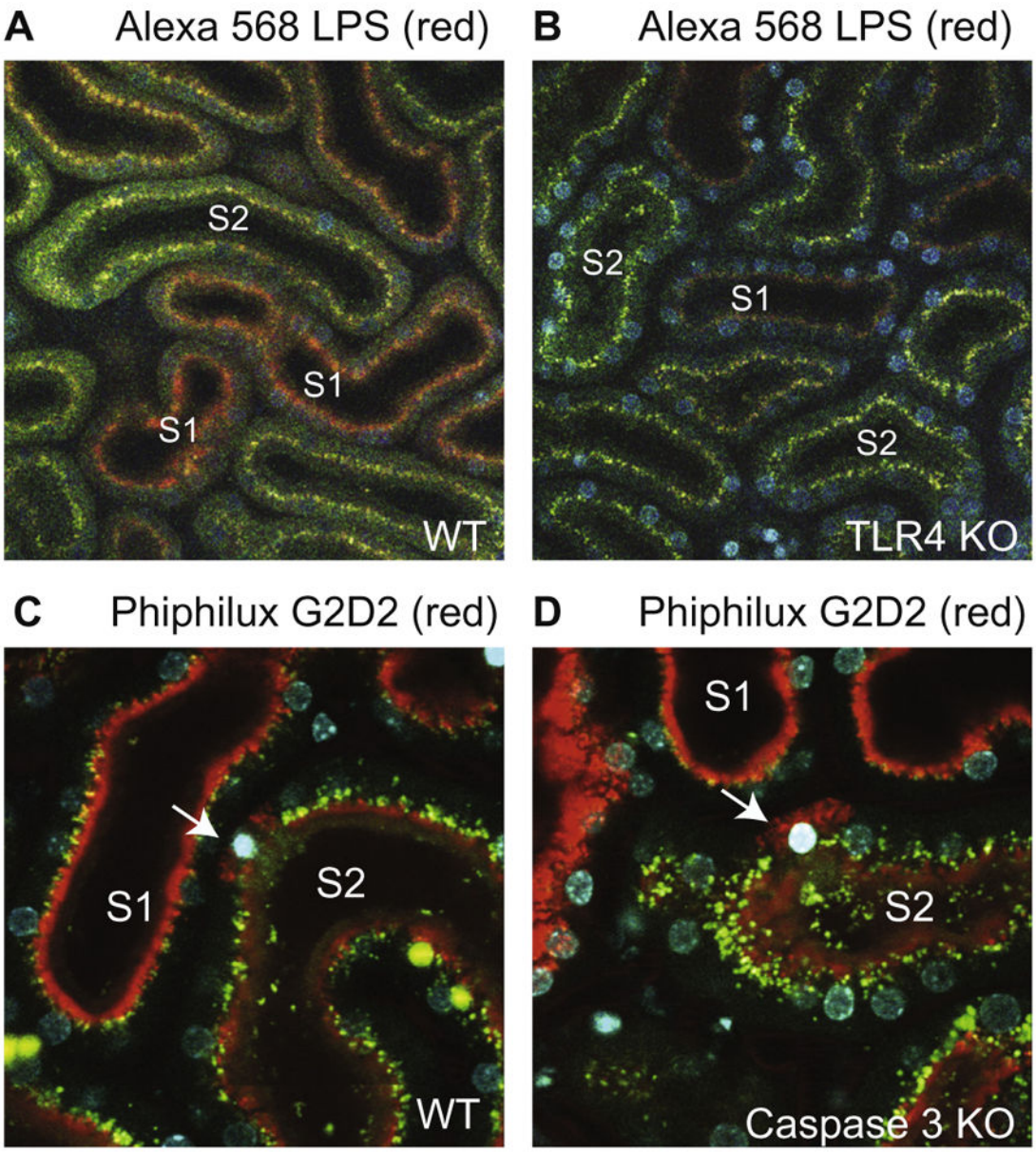

Fig. 3.

Effect of fluid phase uptake and nonspecific probe signal. (A) Systemically administered Alexa 568-labeled LPS (red) is robustly internalized by S1 proximal tubules of wild-type mice. (B) TLR4 knockout mice exhibit mild LPS uptake by S1 via fluid phase endocytosis. Blue is nuclear Hoechst. (C and D) Activated caspase 3 sensor Phiphilux G2D2 (red) is observed primarily in the S1 proximal tubules. No difference was found between wild-type and caspase 3 knockout mice. Arrows point to apoptotic cells where non-specific, caspase-3-independent Phiphilux signal is observed. (For interpretation of the references to colour in this figure legend, the reader is referred to the web version of this article.)

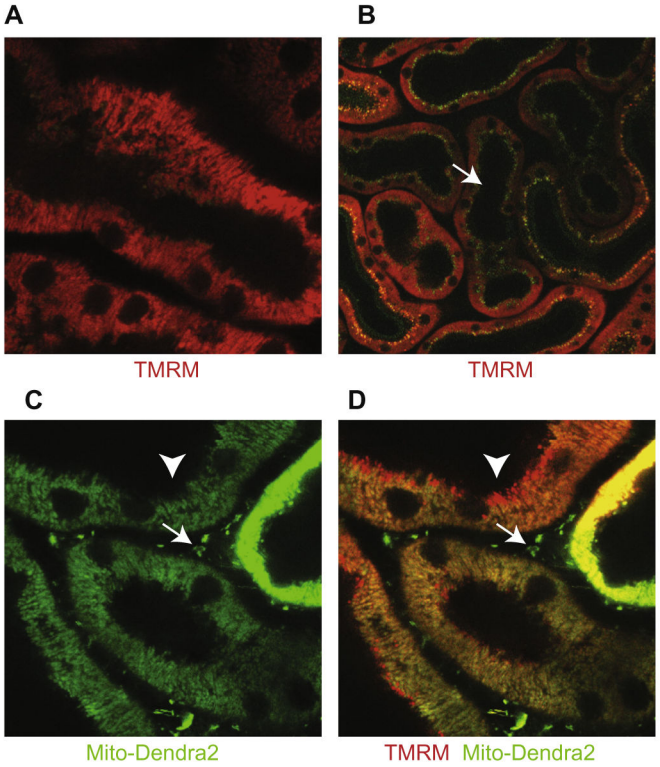

Fig. 4.

Intravital mitochondrial imaging. (A) A magnified view of TMRM signal (red) in proximal tubules of wild-type mouse. TMRM was administered intravenously 20 min before imaging. (B) Arrow points to heterogeneous distribution of TMRM in the renal cortex. (C–D) Intravital imaging of Mito-Dendra2 mouse kidney before and after TMRM administration. Dendra2 is expressed in mitochondria (green; not photo-activated in this experiment). Arrows and arrowheads point to areas that lack colocalization of TMRM and Dendra2. (For interpretation of the references to colour in this figure legend, the reader is referred to the web version of this article.)

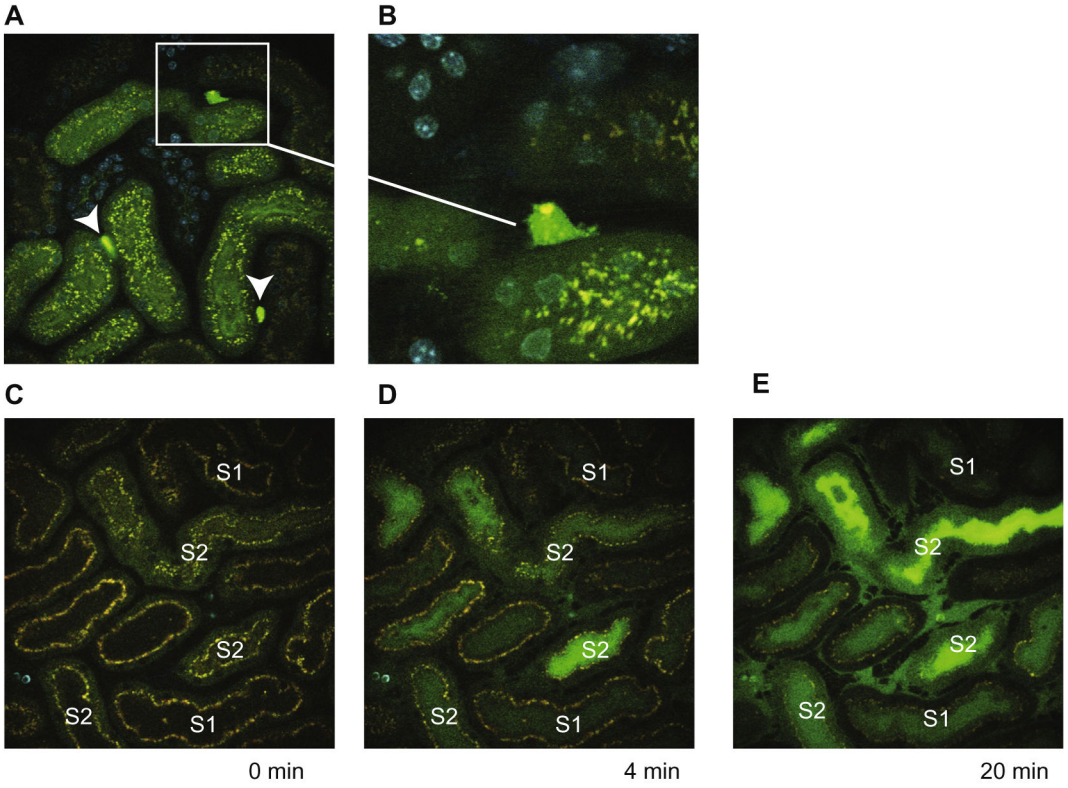

Fig. 5.

Effect of free dye leakage from liposomes. (A and B) Calcein liposomes were administered after removal of the leaked free dye. They were phagocytosed by renal macrophages which then exhibited a bright green calcein signal (90 min after intravenous administration). The green tubular signal represents tubular autofluorescence seen even before calcein administration. (C and D) Calcein liposomes were administered without removing the free dye. Time-lapse imaging shows dye secretion predominantly into the lumen of S2 segments. (For interpretation of the references to colour in this figure legend, the reader is referred to the web version of this article.)

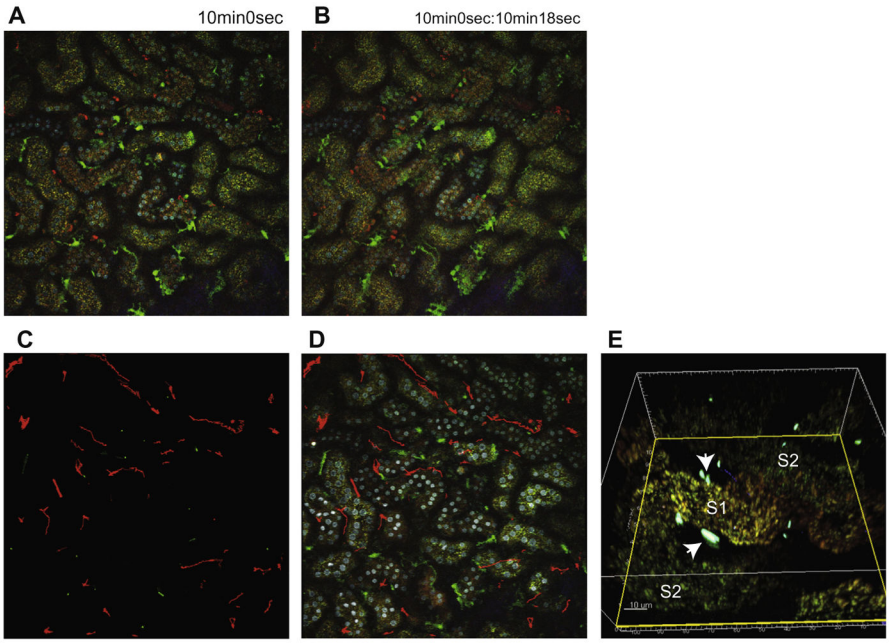

Fig. 6.

Image data processing. (A and B) The CX_3CR1-EGFP mouse (green in myeloid cells) was injected with rhodamine-labeled high-molecular weight poly (I:C; red) and a time-series was obtained every 9 s. Motion artifacts were corrected using IMART (Intravital Microscopy Artifact Reduction Tool). See Supplemental video 3 showing original time-lapse images (left), post rigid registration (middle), and post non-rigid registration (right). (C and D) Time-graded tracking of the poly (I:C) positive cells was performed using a custom plugin for ImageJ [17]. This custom plugin enables tracking of cells with poor cell body delineation and punctate signals by determining the center of mass for a given cell from the punctate staining. (D) Live E coli (cyan; arrows) were injected intravenously and z-stack kidney images were reconstructed with Imaris. (For interpretation of the references to colour in this figure legend, the reader is referred to the web version of this article.)

Table 1

Probe	Characteristic	Reference
Hoechst 33342	Nuclear stain	[1]
Tetramethylrhodamine	Mitochondrial membrane potential	[13,29]
Rhodamine-123	Mitochondrial membrane potential	[5]
H_2DCFDA	Reactive oxygen species	[13,17]
Dihydroethidium	Reactive oxygen species	[13]
Cationic styryl dye (ASP^+)	Organic cation transporter	[46]
Calcein AM	Cell viability	[30]
BCECF	pH	[47]
Sulfonefluorescein	Organic anion secretion	[48]

Fluorescently-tagged probes such as dextran conjugates are not included.

ASP^+, 4-(4-(dimethylamino)styryl)-N-methyl-pyridinium; H_2DCFDA, 2′,7′-dichlorodihydrofluorescein diacetate; BCECF, 2′,7′-bis(2-carboxyethyl)-5(6)-carboxyfluorescein.